Results in Physics 27 (2021) 104369

Contents lists available at ScienceDirect

Results in Physics

journal homepage: www.elsevier.com/locate/rinp

Analytical optical soliton solutions of the Schrödinger-Poisson dynamical system

M. Younis [a], Aly R. Seadawy [b,*], M.Z. Baber [c], S. Husain [c], M.S. Iqbal [c], S.T. R. Rizvi [d], Dumitru Baleanu [e,f,g]

[a] PUCIT, University of the Punjab, Lahore, Pakistan
[b] Department of Mathematics, Faculty of science, Taibah University, Al-Madinah Al-Munawarah, Saudi Arabia
[c] Department of Mathematics and Statistics, The University of Lahorea, Lahore, Pakistan
[d] Department of Mathematics, COMSATS University Islamabad, Lahore Campus, Pakistan
[e] Department of Mathematics, Cankaya University, Ankara, Turkey
[f] Department of Medical Research, China Medical University Hospital, China Medical University, Taichung, Taiwan, Republic of China
[g] Institute of Space Sciences, 077125 Magurele, Romania

ARTICLE INFO

Keywords:
Exact solutions
Schrödinger-Poisson system
Integrability
Modified extended direct algebraic
(G'/G)-expansion

ABSTRACT

The article studies the exact traveling wave solutions to the Schrödinger-Poisson system which has applications in gravity's role of quantum state and approximate the coupling between quantum mechanics with gravitation. Diverse exact solutions in hyperbolic, trigonometric and plane wave forms are obtain using two norms of integration. For this sake modified extended direct algebraic (MEDA) and (G'/G)-expansion techniques are used. The 3D plots and their corresponding contour graphs are also depicted. The constraints conditions for the exact of solutions are also emerged during the derivation of solution.

Introduction

Nonlinear partial differential equations (NPDEs) have been comprehensively studied in recent years. These equations play fundamental role in the modeling of various fields of science and engineering such as solid state physics, thermodynamics, civil engineering, soil mechanics, economics and quantum physics [1–7]. Many nonlinear systems are also emerged in coupled form, and these systems have great important impact in different fields of sciences [1].

Thus in this article, the Schrödinger-Poisson system is under investigation. This system is fundamentally the Schrödinger equation together with the gravitational potential, which has application of gravity's role in quantum state [2]. Also this nonlinear system can approximate the coupling between quantum mechanics with gravitation [3]. Further this system can also be viewed as the junction of Einstein-Klein Gordon and Einstein-Dirac system [4]. MEDA and (G'/G)-expansion methods [8–11] are applied to find the exact solutions to this system to find the exact solutions, has impressive impact in the theory of solitons [12–15]. These types of solutions play multiple significant role in the appropriate understanding of qualitative features of numerous phenomena and processes in different areas of natural science. The Schrödinger-Poisson system is read as

$$\begin{cases} -i\dfrac{\partial\psi}{\partial t} = -\Delta\psi + \phi(x)\psi \\ -\Delta\phi = |\psi|^2 \end{cases} \tag{1}$$

The wave profile function is defined by $\psi(x, t)$. Here, function ϕ is additionally has an elliptic behavior *i.e.*, a solution of Schrödinger-Poisson system. In this case where $\phi(x)$ is determine by charge of the wave function itself. Using the definition of Δ, the last system can be converted into single equation which has the following form,

$$-i\frac{\partial^3\psi}{\partial x^2\partial t} + \frac{\partial^4\psi}{\partial x^4} + 2\phi'(x)\frac{\partial\psi}{\partial x} - \phi(x)\frac{\partial^2\psi}{\partial x^2} + |\psi|^2\psi = 0. \tag{2}$$

Much concentration has been paid to the models of NLPDEs for finding exact solutions in last few years. There are many powerful methods have been constructed and developed to analytically solve NPDEs with the aid of computational software such as Maple, Mathematica and Matlab [5]. The efficiency and reliability of such software is much better. In recent decades, exact solutions [6], analytical solutions [7] and numerical

* Corresponding author.
E-mail address: aabdelalim@taibahu.edu.sa (A.R. Seadawy).

https://doi.org/10.1016/j.rinp.2021.104369
Received 9 March 2021; Received in revised form 20 May 2021; Accepted 21 May 2021
Available online 21 June 2021

solutions [8] of many NPDEs have been successfully obtained [9]. The methods for obtaining exact explicit solutions of NPDEs are the tanh-function method [10], the exp-function method [11], the F-expansion method [16], Hirota method [17], Kudryashov method [9], the MEDA method [18], the extended auxiliary equation method [19] and modified method of simplest equation, the (G'/G^2)-expansion method [20], modified mapping method [21] and extended Fan-sub equation method [22]. Examples of the methods for solving NPDEs numerically are the finite element method [23], finite volume method [24], generalized finite difference method [25], spectral collocation method [26] and Galerkin finite element method [27]; $(G'/G), 1/G)$-expansion method [28]; the unified method [29]; simplified Hirota's method [30]; the exp $(-\Phi(\xi))$ method [31]. Hence, there are results containing the extended and modified direct algebraic method, extended mapping method, and Seadawy technique of valuable researches in which may well complement the existing literature such as [32–39] In the following section, the model is a investigated analytically.

Analysis of Schrödinger-Poisson system

In this section, we adopt two integration norms namely MEDA [40] and (G'/G)-expansion method [41].

Using MEDA-method

Let us find the new exact traveling wave solutions to the system Eq. (1). For this, we convert Eq. (2) into nonlinear ordinary differential equation using the following complex transformation.

$$\psi(x,t) = U(z) \times e^{ip}, \tag{3}$$

where $\psi(x,t)$ is the wave amplitude of wave profile, $z = x - vt$, and x is independent spatial variable and $t$represents the temporal variable, $v$is the velocity of the wave. Also note that $p = p_1 x + p_2 t$, where $p_1$and $p_2$are arbitrary constants. Hence substituting the results of Eq. (3) into Eq. (1) can get the equation, then separating the real and imaginary parts yields a pair of relations. The imaginary part gives the following constraint condition.

$$\rho_1 v = \left(2\phi(x) + 2p_2 + p_1^2\right) \tag{4}$$

and real parts take the form,

$$\begin{aligned} &U^{iv}(z) + \left(2vp_1 - 6p_1^2 - p_2 - \phi(x)\right)U''(z) - 2\left(\phi'\right)(x)U'(z) + \left({p_1}^4 + p_2 p_1^2\right. \\ &\left. + \phi(x)p_1^2\right)U(z) + U^3(z) \\ &= 0. \end{aligned} \tag{5}$$

The value of the positive integer N can be determined using the homogeneous balance principle, *i.e*, by balancing between the highest order derivatives and the nonlinear terms occurring in Eq. (5).

$$N + 4 = 3N \Rightarrow N = 2.$$

Thus, Eq. (5) the formal solutions are obtained using the following result.

$$U(z) = \beta_0 + \beta_1\eta(z) + \beta_2\eta^2(z) + \gamma_1\eta^{-1}(z) + \gamma_2\eta^{-2}(z), \tag{6}$$

where $\beta_0, \beta_1, \beta_2, \gamma_1, \gamma_2$ are unknown constants, and $\eta'(z) = \gamma + \eta^2(z)$ in which γ is a free-parameter. Substituting Eq. (6) into Eq. (5) with the aid of $\eta'(z) = \gamma + \eta^2(z)$, by collecting all the terms with the same power of $\eta(z)$ [42]. After equating each coefficient equal to zero, this yields a set of following algebraic equations. Solving this system of algebraic equations with the aid of maple, we obtained following set of solutions.

For Case-1: The $\beta_2, \gamma_2, v, \gamma$ are free parameters while along with the value of $\beta_0 = 0, \beta_1 = 0, \gamma_1 = 0, \beta_2 = \pm 2\sqrt{-30}$, $\gamma_2 = \pm 2\gamma^2\sqrt{-30}$, $v = \frac{-40\gamma + 6p_1^2 + \phi(x) + p_2}{2p_1}$.The constraint condition hold for the following results, when v is putting in it, $\gamma = -\frac{3}{40}\phi(x) - \frac{3}{40}p_2 + \frac{1}{10}p_1^2$. For $\gamma < 0$, thus following families of hyperbolic solutions are obtained.

$$\begin{aligned} \psi_1 = \Big(&\pm 2, \sqrt{-30}\,(-\sqrt{-\gamma}\tanh(\sqrt{-\gamma}\,z))^2 \\ &\pm 2\gamma^2\sqrt{-30}\,(-\sqrt{-\gamma}\tanh(\sqrt{-\gamma}\,z))^{-2}\Big)e^{ip}, \end{aligned}$$

or

$$\begin{aligned} \psi_2 = \Big(&\pm 2\sqrt{-30}\,(-\sqrt{-\gamma}\coth(\sqrt{-\gamma}\,z))^2 \\ &\pm 2\gamma^2\sqrt{-30}\,(-\sqrt{-\gamma}\coth(\sqrt{-\gamma}\,z))^{-2}\Big)e^{ip}. \end{aligned}$$

For $\gamma > 0$, thus following periodic wave solutions are obtained.

$$\psi_3 = \left(\pm 2\sqrt{-30}\left(\sqrt{\gamma}\tan\left(\sqrt{\gamma}\,z\right)\right)^2 \pm 2\gamma^2\sqrt{-30}\left(\sqrt{\gamma}\tan\left(\sqrt{\gamma}\,z\right)\right)^{-2}\right)e^{ip},$$

or

$$\begin{aligned} \psi_4 = \Big(&\pm 2\sqrt{-30}\left(-\sqrt{\gamma}\cot\left(\sqrt{\gamma}\,z\right)\right)^2 \\ &\pm 2\gamma^2\sqrt{-30}\left(-\sqrt{\gamma}\cot\left(\sqrt{\gamma}\,z\right)\right)^{-2}\Big)e^{ip}. \end{aligned}$$

For $\gamma = 0$, the following plan solutions are obtained.

$$\psi_5 = \left(\pm 2\sqrt{-30} \pm 2\gamma^2\sqrt{-30}\,z^{-2}\right)e^{ip}$$

The graph and its corresponding contour plot of the solutions $\psi_1(x,t)$ are shown in Fig. 1, for the values of parameters $\rho_1 = 0.5, \rho_2 = 0.008$, $\gamma = 0.0005, \phi(x) = sin(x)$ and $\nu = 0.0009$.

The graph and its corresponding contour plot of the solutions $\psi_2(x,t)$ are shown in Fig. 2, for the values of parameters $\rho_1 = 0.5, \rho_2 = 0.008$, $\gamma = 0.0005, \phi(x) = sin(x)$ and $\nu = 0.0009$.

The graph and its corresponding contour plot of the solutions $\psi_4(x,t)$ are shown in Fig. 3, for the values of parameters $\rho_1 = 0.5, \rho_2 = 0.008$, $\gamma = 0.0005, \phi(x) = sin(x)$ and $\nu = 0.0009$.

The graph and its corresponding contour plot of the solutions $\psi_5(x,t)$ are shown in Fig. 4, for the values of parameters $\rho_1 = 0.5, \rho_2 = 0.008$, $\gamma = 0.0005, \phi(x) = sin(x)$ and $\nu = 0.0009$.

For Case-2: The $\gamma_1, \gamma_2, \gamma, v$are free parameters while along with $\beta_0 = 0$, $\beta_1 = 0$, $\beta_2 = 0$, $\gamma_1 = \pm\frac{1}{4}\sqrt{-2}\left(\phi'(x) - \sqrt{512\gamma^3 + (\phi'(x))^2}\right)$, $\gamma_2 = \pm 2\gamma^2\sqrt{-30}$.

$$16p_1\gamma^2 v = 48p_1^2\gamma^2 + (\phi'(x))^2 + 8\phi(x)\gamma^2 - 64\gamma^3 + 8p_2\gamma^2 - \sqrt{512\,(\phi'(x))^2\gamma^3 + (\phi'(x))^4}$$

The constraint condition holds for the following results, when $v$is putting in it, $24\gamma^2\phi(x) = -24p_2\gamma^2 + 32p_1^2\gamma^2 + ((\phi')(x))^2 - 64\gamma^3 - \sqrt{512((\phi')(x))^2\gamma^3 + ((\phi')(x))^4}$,For $\gamma < 0$, thus following families of hyperbolic solutions are obtained.

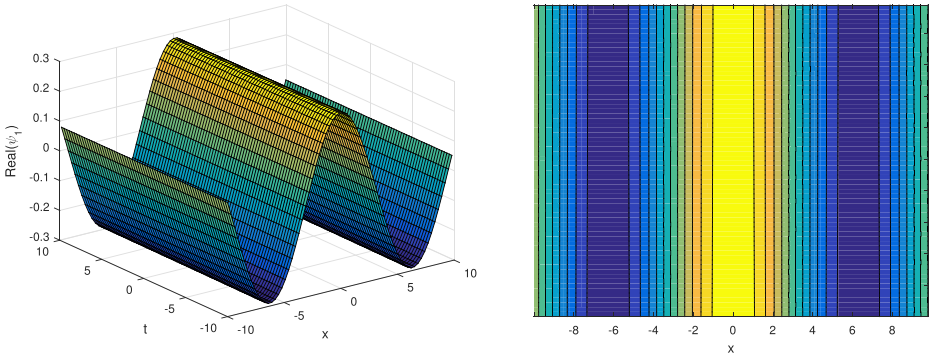

Fig. 1. The 3D plot and the corresponding contour representation of the traveling wave solutions $\psi_1(x,t)$ for different values of parameters.

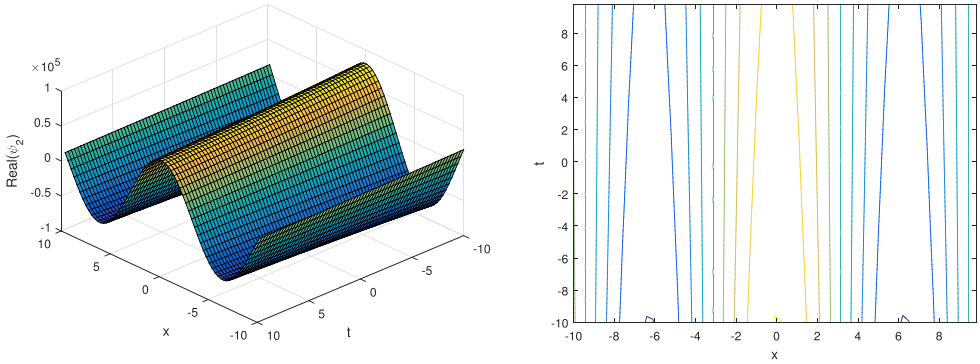

Fig. 2. The 3D plot and the corresponding contour representation of the traveling wave solutions $\psi_2(x,t)$ for different values of parameters.

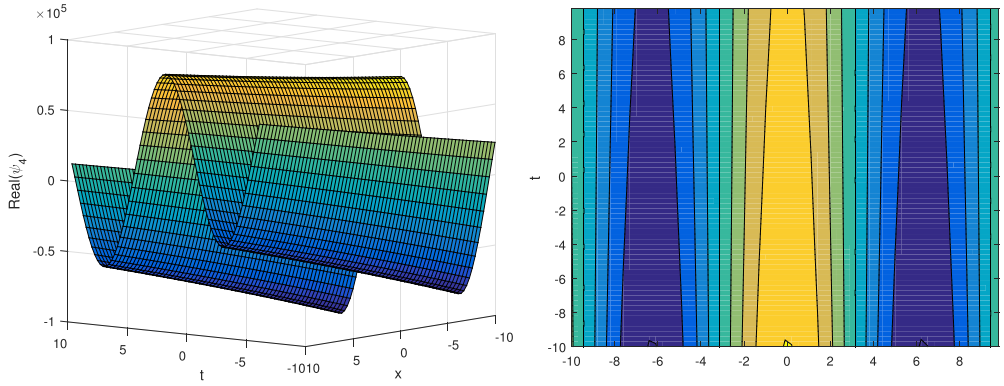

Fig. 3. The 3D plot and the corresponding contour representation of the traveling wave solutions $\psi_4(x,t)$ for different values of parameters.

$$\psi_6 = \left(\left(\pm\frac{\sqrt{-2}\,\phi'(x)}{4} - \sqrt{512\gamma^3 + (\phi'(x)^2)}\,\right)\left(-\sqrt{-\gamma}\tanh(-\sqrt{-\gamma}\,z)\right)^{-1} \pm 2\gamma^2\sqrt{-30}\left(-\sqrt{-\gamma}\tanh(-\sqrt{-\gamma}\,z)\right)^{-2}\right)e^{ip},$$

or

$$\psi_7 = \left(\left(\pm\frac{\sqrt{-2}\,\phi'(x)}{4} - \sqrt{512\gamma^3 + (\phi'(x)^2)}\,\right)\left(-\sqrt{-\gamma}\coth(-\sqrt{-\gamma}\,z)\right)^{-1} \pm 2\gamma^2\sqrt{-30}\left(-\sqrt{-\gamma}\coth(-\sqrt{-\gamma}\,z)\right)^{-2}\right)e^{ip}.$$

For $\gamma > 0$, thus following periodic wave solutions are obtained.

$$\psi_8 = \left(\left(\pm\frac{\sqrt{-2}\,\phi'(x)}{4} - \sqrt{512\gamma^3 + \phi'(x)^2}\,\right)\left(\sqrt{\gamma}\tan\left(\sqrt{\gamma}\,z\right)\right)^{-1} \pm 2\gamma^2\sqrt{-30}\left(\sqrt{\gamma}\tan(\sqrt{\gamma}\,z)\right)^{-2}\right)e^{ip},$$

or

$$\psi_9 = \left(\left(\pm\frac{\sqrt{-2}\,\phi'(x)}{4} - \sqrt{512\gamma^3 + \phi'(x)^2}\,\right)\left(-\sqrt{\gamma}\cot\left(\sqrt{\gamma}\,z\right)\right)^{-1} \pm 2\gamma^2\sqrt{-30}\left(-\sqrt{\gamma}\cot(\sqrt{\gamma}\,z)\right)^{-2}\right)e^{ip}.$$

For $\gamma = 0$, thus following plane solutions are obtained.

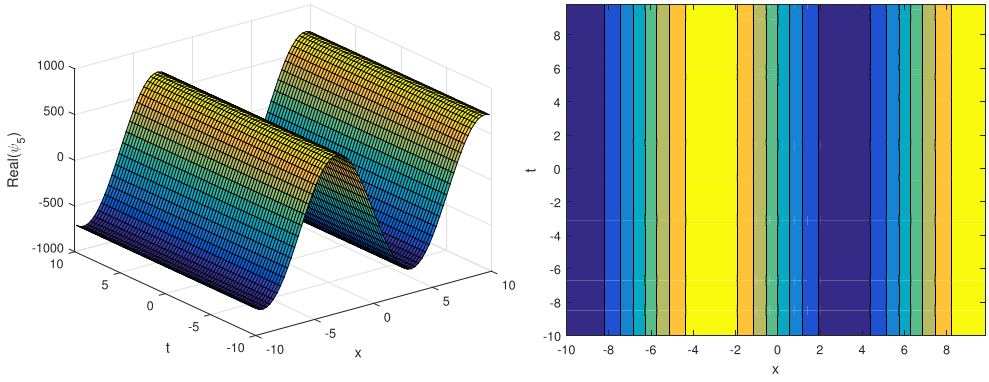

Fig. 4. The 3D plot and the corresponding contour representation of the traveling wave solutions $\psi_5(x,t)$ for different values of parameters.

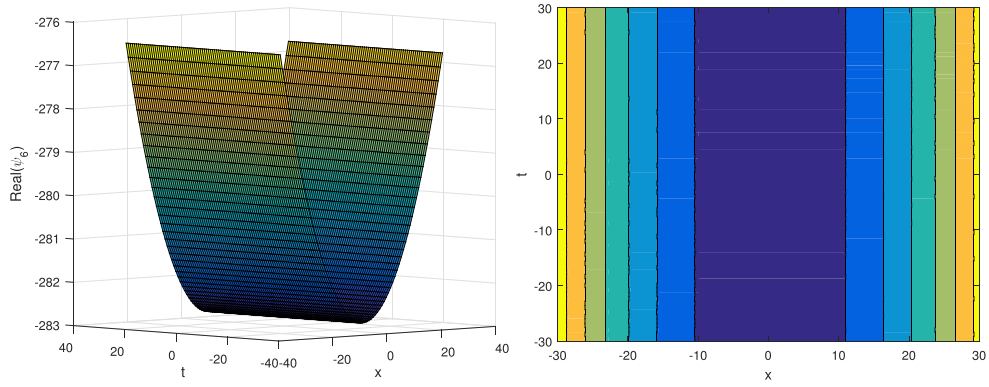

Fig. 5. The 3D plot and the corresponding contour representation of the traveling wave solutions $\psi_6(x,t)$ for different values of parameters.

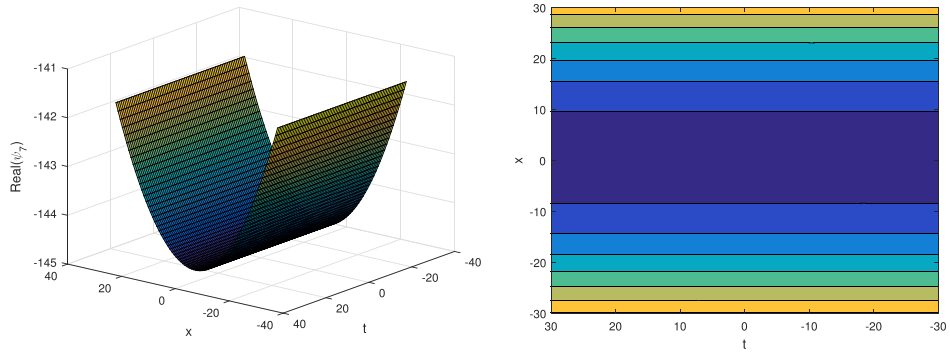

Fig. 6. The 3D plot and the corresponding contour representation of the traveling wave solutions $\psi_7(x,t)$ for different values of parameters.

$$\psi_{10}=\left(\left(\pm\frac{\sqrt{-2}\,\phi'(x)}{4}-\sqrt{512\gamma^3+\phi'(x)^2}((-z^{-1}))\pm 2\gamma^2\sqrt{-30}\,z^{-2}\right)e^{ip}\right.$$

The graphs and its corresponding contours plot of the solutions $\psi_6(x,t)$ are shown in Fig. 5, for the values of parameters $\rho_1=0.007,\rho_2=0.08,\gamma=0.005,\phi(x)=sin(x)$ and $\nu=0.0019$.

The graphs and its corresponding contour plot of the solutions $\psi_7(x,t)$are shown in Fig. 6, for the values of parameters $\rho_1=0.007,\rho_2=0.08,\gamma=0.005,\phi(x)=sin(x)$and $\nu=0.0019$.

The graphs and its corresponding contour plot of the solutions $\psi_8(x,t)$ are shown in Fig. 7, for the values of parameters $\rho_1=0.007,\rho_2=0.08,\gamma=0.005,\phi(x)=sin(x)$and $\nu=0.0019$.

For Case-3: The $\beta_2,\gamma_1,\nu,\gamma$are free parameters while along with $\gamma_2=0$, $\beta_0=0$, $\beta_1=0$, $\beta_2=\pm2\sqrt{-30}$, $\gamma_1=\pm\sqrt{-40\gamma-4\nu p_1+12p_1^2+2\phi(x)+2p_2}$, $2p_1\nu=-40\gamma+6p_1^2+\phi(x)+p_2$, $\gamma=\frac{1}{8}\sqrt{p_1^2+p_2+\phi(x)}p_1$,The constraint condition holds for the following results, when $\nu$is putting in it, $\gamma=-\frac{3}{40}\phi(x)-\frac{3}{40}p_2+\frac{1}{10}p_1^2$.

For $\gamma<0$, thus following families of hyperbolic solutions are obtained.

$$\psi_{11}=\left(\pm2\sqrt{-30}(-\sqrt{-\gamma}\tanh(\sqrt{-\gamma}z))^2\right.$$
$$\left.\pm\sqrt{-40\gamma-4\nu p_1+12p_1^2+2\phi(x)+2p_2}(-\sqrt{-\gamma}\tanh(\sqrt{-\gamma}z))^{-1}\right)e^{ip},$$

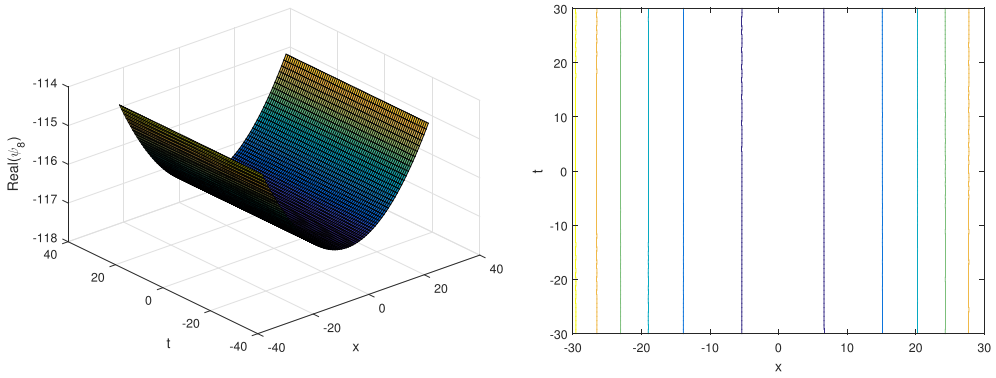

Fig. 7. The 3D plot and the corresponding contour representation of the traveling wave solutions $\psi_8(x,t)$ for different values of parameters.

or

$$\psi_{12}=\left(\pm 2\sqrt{-30}\,(-\sqrt{-\gamma}\coth(\sqrt{-\gamma}\,z))^2 \pm\sqrt{-40\gamma-4\nu p_1+12p_1^2+2\phi(x)+2p_2}\,(-\sqrt{-\gamma}\coth(\sqrt{-\gamma}\,z))^{-1}\right)e^{ip}.$$

For $\gamma>0$, thus following periodic wave solutions are obtained.

$$\psi_{13}=\left(\pm 2\sqrt{-30}\,(\sqrt{\gamma}\tan\left(\sqrt{\gamma}\,z\right))^2 \pm\sqrt{-40\gamma-4\nu p_1+12p_1^2+2\phi(x)+2p_2}\,(\sqrt{\gamma}\tan\left(\sqrt{\gamma}\,z\right))^{-1}\right)e^{ip},$$

t) are shown in Fig. 10, for the values of parameters $\rho_1=1.1,\rho_2=0.0002,\gamma=0.001,\phi(x)=sin(x)$ and $\nu=0.001$.

The graph and its corresponding contour plot of the solutions $\psi_{15}(x,t)$ are shown in Fig. 11, for the values of parameters $\rho_1=1.1,\rho_2=0.0002,\gamma=0.001,\phi(x)=sin(x)$ and $\nu=0.001$.

For Case-4: The $\beta_0,\beta_2,\gamma_2,\nu$, are free parameters while along with $\gamma_1=0,\ \beta_1=0,\ \beta_2=\pm2\sqrt{-30},\ \beta_0=\pm4\frac{\phi'(x)\left(2\sqrt{-30}\right)}{p_1^4},\ \gamma_2=\frac{\gamma\left(\phi(x)p_1^{10}-184\gamma^2p_1^8+p_2p_1^{10}+6\sqrt{-30}p_1^8+p_1^{12}+48\left(\phi'(x)\left(2\sqrt{-30}\right)\right)^2\right)}{16(p_1{}^4\phi'(x)\left(2\sqrt{-30}\right))},\ \gamma=-\frac{-6p_1^6-\phi(x)p_1^4-p_2p_1^4+4\sqrt{-30}\phi'(x)\left(2\sqrt{-30}\right)+2\nu p_1^5}{40p_1^4}$

$$16p_1^9\gamma\nu=-\phi(x)p_1^{10}+136\gamma^2p_1^8-8\phi(x)\gamma p_1^8-8p_2\gamma p_1^8+p_2p_1^{10}+6\sqrt{-30}p_1^8+p_1^{12}-48p_1^{10}\gamma+48\left(\phi'(x)\left(2\sqrt{30}\right)\right)^2$$

or

$$\psi_{14}=\left(\pm 2\sqrt{-30}\,(-\sqrt{\gamma}\cot\left(\sqrt{\gamma}\,z\right))^2 \pm\sqrt{-40\gamma-4\nu p_1+12p_1^2+2\phi(x)+2p_2}\,(-\sqrt{\gamma}\cot\left(\sqrt{\gamma}\,z\right))^{-1}\right)e^{ip}.$$

For $\gamma=0$, thus following plane solutions are obtained.

$$\psi_{15}=\left(\pm 2\sqrt{-30}\,z^{-2}\pm\sqrt{-40\gamma-4\nu p_1+12p_1^2+2\phi(x)+2p_2}\,(-z^{-1})\right)e^{ip}$$

The graph and the corresponding contour plot of the solutions $\psi_{11}(x,t)$ are shown in Fig. 8, for the values of parameters $\rho_1=1.1,\rho_2=0.0002,\gamma=0.001,\phi(x)=sin(x)$ and $\nu=0.001$

The graph and the corresponding contour plot of the solutions $\psi_{12}(x,t)$ are shown in Fig. 9, for the values of parameters $\rho_1=1.1,\rho_2=0.0002,\gamma=0.001,\phi(x)=sin(x)$ and $\nu=0.001$.

The graph and its corresponding contour plot of the solutions $\psi_{14}(x,$

The constraint condition holds for the following results, when $\nu$is putting in it,

$$\gamma=\frac{\left(8p_1^6-6p_1^4p_2-6p_1^4\phi(x)-\sqrt{\alpha_1+\alpha_2}\right)}{68p_1^4}$$

where

$$\alpha_1=-30p_1^{12}+130p_2p_1^{10}+130\phi(x)p_1^{10}-36p_1^8p_2^2-72p_1^8p_2\phi(x)-36p_1^8\phi^2(x)$$

$$\alpha_2=204\sqrt{-30}p_1^8+1632\left(\phi(x)\left(2\sqrt{-30}\right)\right)^2$$

For $\gamma<0$, thus following families of hyperbolic wave solutions are obtained.

$$\psi_{16}=\left(\pm\frac{8\phi'(x)\left(\sqrt{-30}\right)}{p_1^4}\pm2\sqrt{-30}\,(-\sqrt{-\gamma}\tanh(\sqrt{-\gamma}\,z))^2 \pm\frac{\gamma\left(\phi(x)p_1^{10}-184\gamma^2p_1^8+p_2p_1^{10}+6sqrt-30p_1^8+p_1^{12}+48\left(\phi'(x)\left(2\sqrt{-30}\right)\right)^2\right)}{16(p_1{}^4\phi'(x)\left(2\sqrt{-30}\right))}(-\sqrt{-\gamma}\tanh\sqrt{-\gamma}\,z)^{-2}\right)e^{ip},$$

or

$$\psi_{17} = \left(\pm \frac{8\phi'(x)\left(\sqrt{-30}\right)}{p_1^4} \pm 2\sqrt{-30}\left(-\sqrt{-\gamma}\coth(\sqrt{-\gamma}\,z)\right)^2 \right.$$
$$\left. \pm \frac{\gamma\left(\phi(x)p_1^{10} - 184\gamma^2 p_1^8 + p_2 p_1^{10} + 6sqrt - 30p_1^8 + p_1^{12} + 48\left(\phi'(x)\left(2\sqrt{-30}\right)\right)^2\right)}{16(p_1{}^4\phi'(x)\left(2\sqrt{-30}\right))}\left(-\sqrt{-\gamma}\coth\sqrt{-\gamma}\,z\right)^{-2} \right) e^{ip}.$$

For $\gamma > 0$, thus following periodic wave solutions are obtained.

$$\psi_{18} = \left(\pm \frac{8\phi'(x)\left(\sqrt{-30}\right)}{p_1^4} \pm 2\sqrt{-30}\left(-\sqrt{-\gamma}\tan(\sqrt{-\gamma}\,z)\right)^2 \right.$$
$$\left. \pm \frac{\gamma\left(\phi(x)p_1^{10} - 184\gamma^2 p_1^8 + p_2 p_1^{10} + 6sqrt - 30p_1^8 + p_1^{12} + 48\left(\phi'(x)\left(2\sqrt{-30}\right)\right)^2\right)}{16(p_1{}^4\phi'(x)\left(2\sqrt{-30}\right))}\left(-\sqrt{-\gamma}\tan\sqrt{-\gamma}\,z\right)^{-2} \right) e^{ip},$$

or

$$\psi_{19} = \left(\pm \frac{8\phi'(x)\left(\sqrt{-30}\right)}{p_1^4} \pm 2\sqrt{-30}\left(-\sqrt{-\gamma}\cot(\sqrt{-\gamma}\,z)\right)^2 \right.$$
$$\left. \pm \frac{\gamma\left(\phi(x)p_1^{10} - 184\gamma^2 p_1^8 + p_2 p_1^{10} + 6sqrt - 30p_1^8 + p_1^{12} + 48\left(\phi'(x)\left(2\sqrt{-30}\right)\right)^2\right)}{16(p_1{}^4\phi'(x)\left(2\sqrt{-30}\right))}\left(-\sqrt{-\gamma}\cot\sqrt{-\gamma}\,z\right)^{-2} \right) e^{ip}.$$

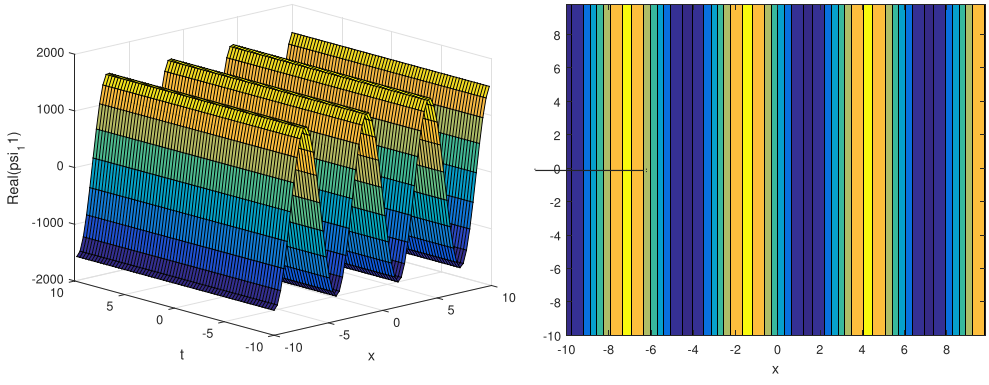

Fig. 8. The 3D plot and the corresponding contour representation of the traveling wave solutions $\psi_{11}(x,t)$ for different values of parameters.

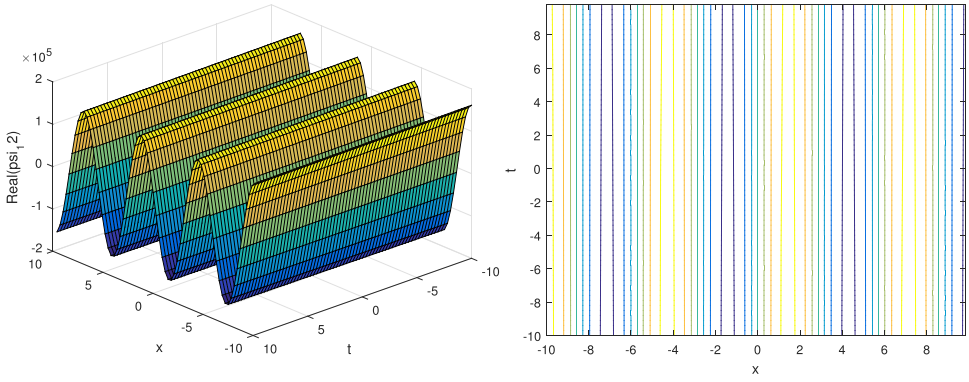

Fig. 9. The 3D plot and the corresponding contour representation of the traveling wave solutions $\psi_{12}(x,t)$ for different values of parameters.

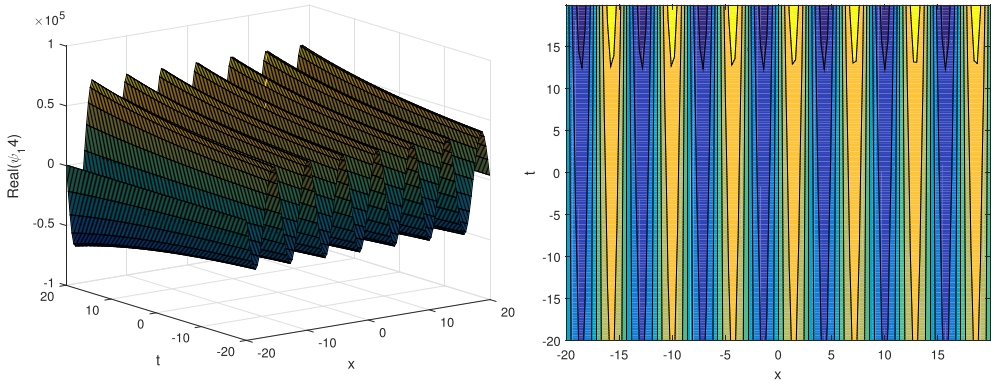

Fig. 10. The 3D plot and the corresponding contour representation of the traveling wave solutions $\psi_{14}(x,t)$ for different values of parameters.

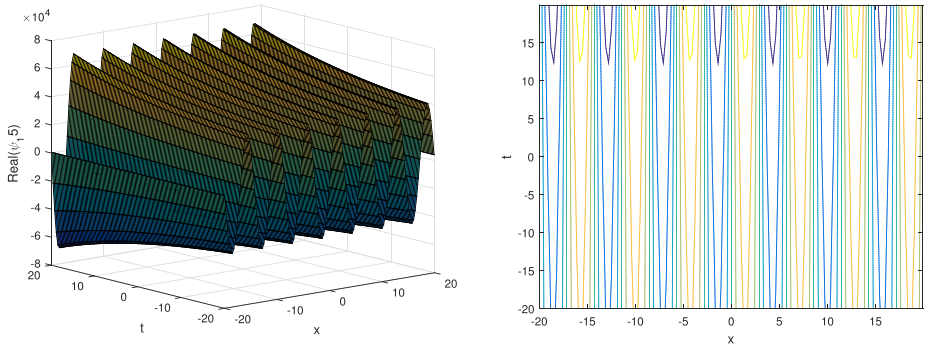

Fig. 11. The 3D plot and the corresponding contour representation of the traveling wave solutions $\psi_{15}(x,t)$ for different values of parameters.

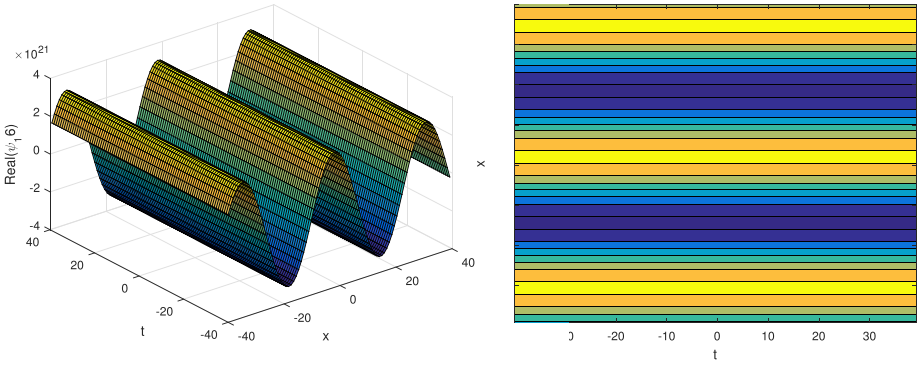

Fig. 12. The 3D plot and the corresponding contour representation of the traveling wave solutions $\psi_{16}(x,t)$ for different values of parameters.

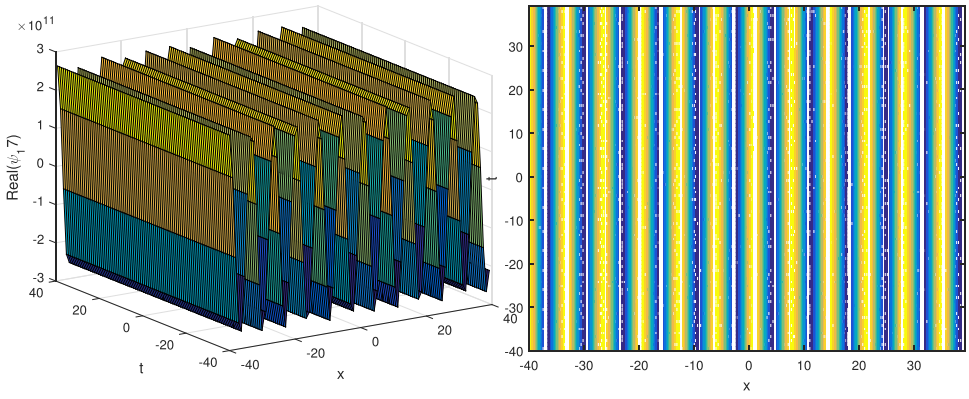

Fig. 13. The 3D plot and the corresponding contour representation of the traveling wave solutions $\psi_{17}(x,t)$ for different values of parameters.

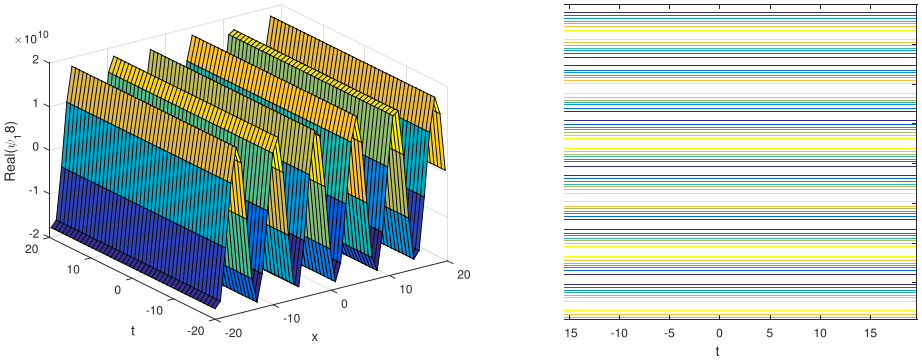

Fig. 14. The 3D plot and the corresponding contour representation of the traveling wave solutions $\psi_{18}(x,t)$ for different values of parameters.

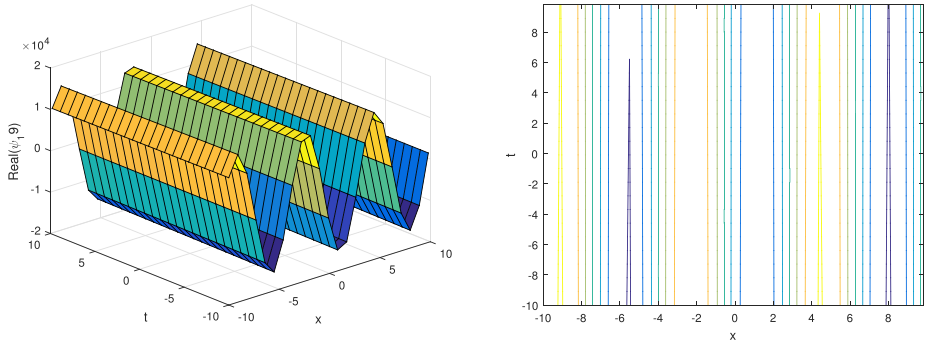

Fig. 15. The 3D plot and the corresponding contour representation of the traveling wave solutions $\psi_{19}(x,t)$ for different values of parameters.

For $\gamma = 0$, thus following plane solutions are obtained.

$$\psi_{20} = \left(\pm \frac{8\phi'(x)\left(\sqrt{-30}\right)}{p_1^4} \pm 2\sqrt{-30}\, z^{-2} \pm \frac{\gamma\left(\phi(x)p_1^{10} - 184\gamma^2 p_1^8 + p_2 p_1^{10} + 6sqrt - 30p_1^8 + p_1^{12} + 48\left(\phi'(x)\left(2\sqrt{-30}\right)\right)^2\right)}{16({p_1}^4\phi'(x)\left(2\sqrt{-30}\right))} z^{-2} \right) e^{ip}$$

The graph and its corresponding contour plot of the solutions $\psi_{16}(x,t)$ are shown in Fig. 12, for the values of parameters $\rho_1 = 0.9190, \rho_2 = 1000.08, \gamma = 0.005, \phi(x) = e^x$ and $\nu = 0.005$

The graph and its corresponding contour plot of the solutions $\psi_{17}(x,t)$ are shown in Fig. 13, for the values of parameters $\rho_1 = 0.9190, \rho_2 = 1000.08, \gamma = 0.005, \phi(x) = e^x$ and $\nu = 0.005$.

The graph and its corresponding contour plot of the solutions $\psi_{18}(x,$

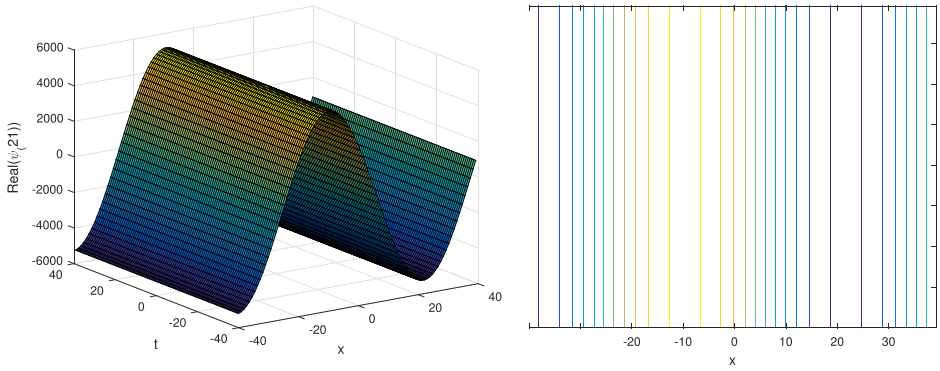

Fig. 16. The 3D plot and the corresponding contour representation of the traveling wave solutions $\psi_{21}(x,t)$ for different values of parameters.

t) are shown in Fig. 14, for the values of parameters $\rho_1 = 0.9190, \rho_2 = 1000.08, \gamma = 0.005, \phi(x) = e^x$ and $\nu = 0.005$.

The graph and its corresponding contour plot of the solutions $\psi_{19}(x, t)$ are shown in Fig. 15, for the values of parameters $\rho_1 = 0.9190, \rho_2 = 1000.08, \gamma = 0.005, \phi(x) = e^x$ and $\nu = 0.005$.

For Case-5: The $\gamma_2, \beta_0, v$are free parameters while along with $\beta_1 = 0$, $\beta_2 = 0, \gamma_1 = 0$,

$$\gamma_2 = \frac{1}{9}\frac{\sqrt{24\phi(x)\gamma - 3p_1^4 - 48vp_1\gamma + 144p_1^2\gamma - 408\gamma^2 + 24p_2\gamma - 3\phi(x)p_1^2 - 3p_2p_1^2}\times\alpha_1}{-2vp_1 + 6p_1^2 + \phi(x) + p_2 - 8\gamma},$$

where

$$\alpha_1 = \left(4\phi(x)\gamma + p_1^4 - 8\,vp_1\gamma + 24p_1^2\gamma - 68\gamma^2 + 4p_2\gamma + \phi(x)p_1^2 + p_2p_1^2\right)$$

$$\gamma_2 = \frac{1}{9}\frac{\sqrt{24\phi(x)\gamma - 3p_1^4 - 48vp_1\gamma + 144p_1^2\gamma - 408\gamma^2 + 24p_2\gamma - 3\phi(x)p_1^2 - 3p_2p_1^2}\times\alpha_1}{-2vp_1 + 6p_1^2 + \phi(x) + p_2 - 8\gamma},$$

where

$$\alpha_1 = \left(4\phi(x)\gamma + p_1^4 - 8\,vp_1\gamma + 24p_1^2\gamma - 68\gamma^2 + 4p_2\gamma + \phi(x)p_1^2 + p_2p_1^2\right)$$

$$\beta_0 = 1\Big/3\sqrt{24\phi(x)\gamma - 3p_1^4 - 48vp_1\gamma + 144p_1^2\gamma - 408\gamma^2 + 24p_2\gamma - 3\phi(x)p_1^2 - 3p_2p_1^2},$$

$$v = 1\Big/14p_1^4 + 3p_1^2\gamma + 1\Big/14p_2p_1^2 + 1\Big/14\phi(x)p_1^2 - 4\gamma^2 + 1\Big/2\phi(x)\gamma + 1\Big/2p_2\gamma - \frac{3}{28p_1\gamma}\{56\gamma^2\phi(x)p_1^2 + 56\gamma^2p_1^4 + 4\phi(x)p_1^6 + 4p_2p_1^4\phi(x) + 2\,(\phi(x))^2p_1^4$$
$$+4p_2p_1^6 + 2p_2^2p_1^4 - 4032\gamma^4 + 2p_1^8 + 56\gamma^2p_2p_1^2\}^{1/2}$$

$$\beta_0 = 1\Big/3\sqrt{24\phi(x)\gamma - 3p_1^4 - 48vp_1\gamma + 144p_1^2\gamma - 408\gamma^2 + 24p_2\gamma - 3\phi(x)p_1^2 - 3p_2p_1^2},$$

For Case-5: The $\gamma_2, \beta_0, v$are free parameters while along with $\beta_1 = 0$, $\beta_2 = 0, \gamma_1 = 0$,

For $\gamma < 0$, thus following families of hyperbolic wave solutions are obtained.

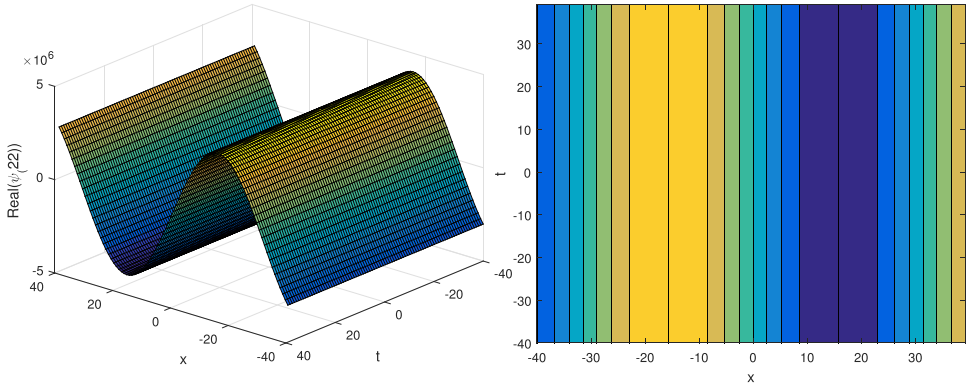

Fig. 17. The 3D plot and the corresponding contour representation of the traveling wave solutions $\psi_{22}(x,t)$ for different values of parameters.

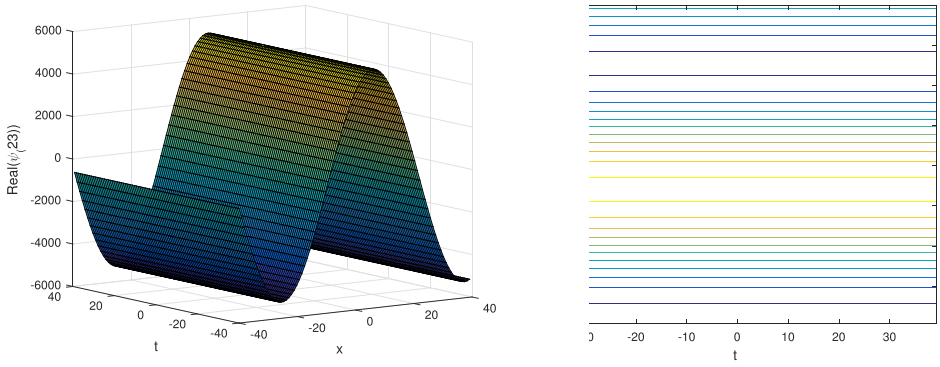

Fig. 18. The 3D plot and the corresponding contour representation of the traveling wave solutions $\psi_{23}(x,t)$ for different values of parameters.

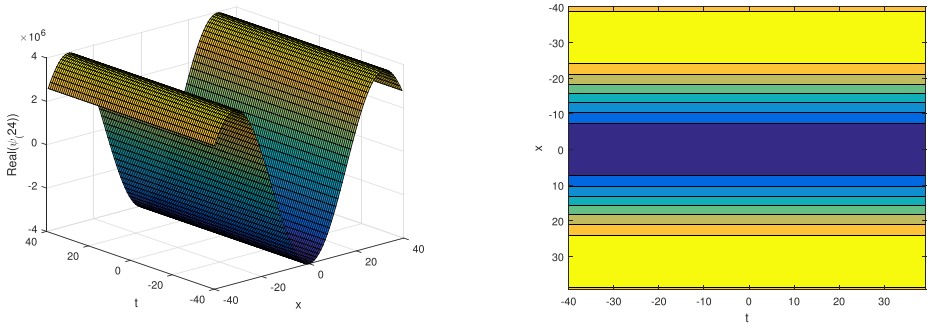

Fig. 19. The 3D plot and the corresponding contour representation of the traveling wave solutions $\psi_{24}(x,t)$ for different values of parameters.

$$\psi_{21}=\left\{\pm 1\Big/\sqrt{24\phi(x)\gamma-3p_1^4-48vp_1\gamma+144p_1^2\gamma-408\gamma^2+24p_2\gamma-3\phi(x)p_1^2-3p_2p_1^2}\right.$$
$$\left.\pm\frac{1}{9}\frac{\sqrt{24\phi(x)\gamma-3p_1^4-48vp_1\gamma+144p_1^2\gamma-408\gamma^2+24p_2\gamma-3\phi(x)p_1^2-3p_2p_1^2}\times\alpha_1}{-2vp_1+6p_1^2+\phi(x)+p_2-8\gamma}(-\sqrt{-\gamma}\tanh(\sqrt{-\gamma}z))^{-2}\right\}e^{ip},$$

or

$$\psi_{22}=\left\{\pm 1\Big/\sqrt{24\phi(x)\gamma-3p_1^4-48vp_1\gamma+144p_1^2\gamma-408\gamma^2+24p_2\gamma-3\phi(x)p_1^2-3p_2p_1^2}\right.$$
$$\left.\pm\frac{1}{9}\frac{\sqrt{24\phi(x)\gamma-3p_1^4-48vp_1\gamma+144p_1^2\gamma-408\gamma^2+24p_2\gamma-3\phi(x)p_1^2-3p_2p_1^2}\times\alpha_1}{-2vp_1+6p_1^2+\phi(x)+p_2-8\gamma}(-\sqrt{-\gamma}\coth(\sqrt{-\gamma}z))^{-2}\right\}e^{ip}.$$

For $\gamma>0$, thus following periodic wave solutions are obtained.

$$\psi_{23}=\left\{\pm 1\Big/\sqrt{24\phi(x)\gamma-3p_1^4-48vp_1\gamma+144p_1^2\gamma-408\gamma^2+24p_2\gamma-3\phi(x)p_1^2-3p_2p_1^2}\right.$$
$$\left.\pm\frac{1}{9}\frac{\sqrt{24\phi(x)\gamma-3p_1^4-48vp_1\gamma+144p_1^2\gamma-408\gamma^2+24p_2\gamma-3\phi(x)p_1^2-3p_2p_1^2}\times\alpha_1}{-2vp_1+6p_1^2+\phi(x)+p_2-8\gamma}(-\sqrt{-\gamma}\tan(\sqrt{-\gamma}z))^{-2}\right\}e^{ip},$$

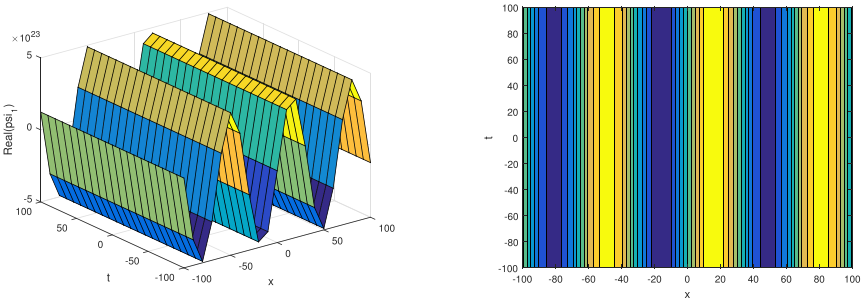

Fig. 20. The 3D plot and the corresponding contour representation of the traveling wave solutions $\psi_1(x,t)$ for different values of parameters.

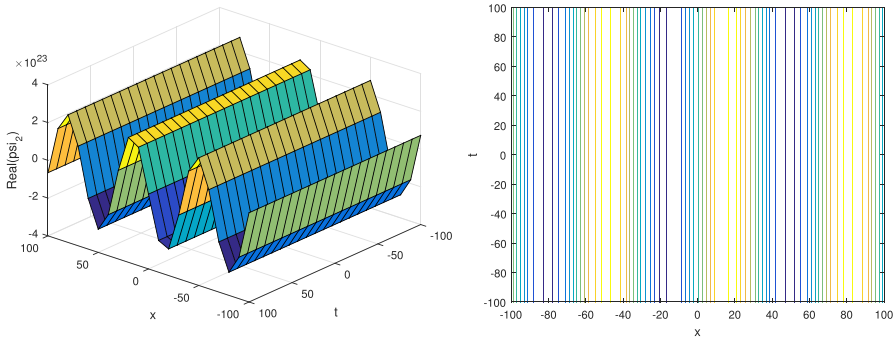

Fig. 21. The 3D plot and the corresponding contour representation of the traveling wave solutions $\psi_2(x,t)$ for different values of parameters.

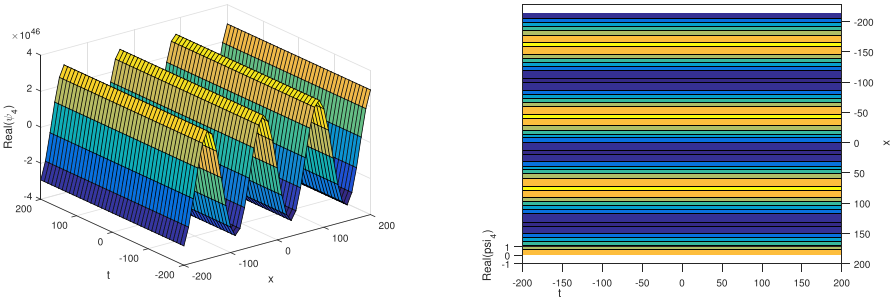

Fig. 22. The 3D plot and the corresponding contour representation of the traveling wave solutions $\psi_4(x,t)$ for different values of parameters.

or

$$\psi_{24} = \left\{ \pm 1 \Big/ 3\sqrt{24\phi(x)\gamma - 3p_1^4 - 48vp_1\gamma + 144p_1^2\gamma - 408\gamma^2 + 24p_2\gamma - 3\phi(x)p_1^2 - 3p_2p_1^2} \right.$$
$$\left. \pm \frac{1}{9}\frac{\sqrt{24\phi(x)\gamma - 3p_1^4 - 48vp_1\gamma + 144p_1^2\gamma - 408\gamma^2 + 24p_2\gamma - 3\phi(x)p_1^2 - 3p_2p_1^2}\times\alpha_1}{-2vp_1 + 6p_1^2 + \phi(x) + p_2 - 8\gamma}\left(-\sqrt{-\gamma}\,cot\left(\sqrt{-\gamma}\,z\right)\right)^{-2} \right\} e^{ip}.$$

For $\gamma = 0$, thus following plane solutions are obtained.

$$\psi_{25} = \left\{ \pm 1 \Big/ 3\sqrt{24\phi(x)\gamma - 3p_1^4 - 48vp_1\gamma + 144p_1^2\gamma - 408\gamma^2 + 24p_2\gamma - 3\phi(x)p_1^2 - 3p_2p_1^2} \right.$$
$$\left. \pm \frac{1}{9}\frac{\sqrt{24\phi(x)\gamma - 3p_1^4 - 48vp_1\gamma + 144p_1^2\gamma - 408\gamma^2 + 24p_2\gamma - 3\phi(x)p_1^2 - 3p_2p_1^2} \times \alpha_1}{-2vp_1 + 6p_1^2 + \phi(x) + p_2 - 8\gamma}(-z^-2) \right\} e^{ip}$$

The graph and its corresponding contour plot of the solutions $\psi_{21}(x, t)$ are shown in Fig. 16, for the values of parameters $\rho_1 = 0.1, \rho_2 = 2, \gamma = 0.005, \phi(x) = sin(x)$ and $\nu = 0.009$

The graph and its corresponding contour plot of the solutions $\psi_{22}(x, t)$ are shown in Fig. 17, for the values of parameters $\rho_1 = 0.1, \rho_2 = 2, \gamma = 0.005, \phi(x) = sin(x)$ and $\nu = 0.009$.

The graph and its corresponding contour plot of the solutions $\psi_{23}(x, t)$ are shown in Fig. 18, for the values of parameters $\rho_1 = 0.1, \rho_2 = 2, \gamma = 0.005, \phi(x) = sin(x)$ and $\nu = 0.009$.

The graph and its corresponding contour plot of the solutions $\psi_{24}(x, t)$ are shown in Fig. 19, for the values of parameters $\rho_1 = 0.1, \rho_2 = 2, \gamma = 0.005, \phi(x) = sin(x)$ and $\nu = 0.009$.

Using $\left(\frac{G'}{G}\right)$*-expansion method*

$$v = \frac{1}{6(4\mu - \lambda^2)p_1}\left(12\phi(x)\mu - 3\phi(x)\lambda^2 + 18p_1^2\lambda^2 - 3p_2p_1^2 + 12p_2\mu - 3p_2\lambda^2 + 3 - 72p_1^2\mu + 3p_1^4 + 3\phi(x)p_1^2 - \left(9 - 18p_2p_1^2 + 18\phi(x)p_1^2 + 48\mu(\phi'(x))^2 - 12\lambda^2(\phi'(x))^2 - 18p_1^6p_2 + 9p_1^4(\phi(x))^2 + 18p_1^6\phi(x) + 9p_1^4p_2^2 + 9p_1^8 - 18p_1^4\phi(x)p_2 + 18p_1^4\right)^{1/2}\right)$$

The constraint condition holds for the following results, when $v$is putting in it,

$$\lambda = -\frac{\sqrt{1728p_1^2p_2\mu - 54p_2 + 2304p_1^4\mu + 90p_1^4p_2 - 54\phi(x) + \alpha_1 + 648\phi(x)\mu p_2}}{3\phi(x) + 8p_1^2 + 3p_2},$$

where

$$\alpha_1 = 1728\phi(x)\mu p_1^2 + 324p_2^2\mu - 54p_1^2\phi(x)^2 - 144p_1^6 + 54p_2^2p_1^2 - 12(\phi'(x))^2 - 144p_1^2 + 324(\phi(x))^2\mu - 198p_1^4\phi(x)$$

The solution of Eq. (5) has the formal solutions of the following form.

$$U(z) = \beta_0 + \beta_1\left(\frac{G'(z)}{G(z)}\right) + \beta_2\left(\frac{G'(z)}{G(z)}\right)^2, \tag{7}$$

Differentiating Eq. (7) w.r.t $z$and then putting $G''(z) + \lambda G'(z) + \mu G(z) = 0$.

After equating each coefficient equal to zero, this yields a set of following algebraic equations. For Case-1: The $v$is free parameter while along with $\beta_2 = 0$, $\beta_1 = \pm\sqrt{-2\phi(x) + 4vp_1 - 2p_2 + 12p_1^2}$,

$$\beta_0 = \pm\frac{\sqrt{-2\phi(x) + 4vp_1 - 2p_2 + 12p_1^2}\left(3\phi(x)\lambda - 18p_1^2\lambda - 6vp_1\lambda + 3p_2\lambda - 2\phi'(x)\right)}{6\phi(x) - 12vp_1 + 6p_2 - 36p_1^2}$$

(i) When $\lambda^2 - 4\mu > 0$thus following hyperbolic solutions are obtained.

$$\psi_1(x,t) = \left\{ \frac{\sqrt{-2\phi(x) + 4vp_1 - 2p_2 + 12p_1^2}\left(3\phi(x)\lambda - 18p_1^2\lambda - 6vp_1\lambda + 3p_2\lambda - 2\phi'(x)\right)}{6\phi(x) - 12vp_1 + 6p_2 - 36p_1^2} + \sqrt{-2\phi(x) + 4vp_1 - 2p_2 + 12p_1^2} \times \left(-\frac{\lambda}{2} + \frac{\sqrt{\lambda^2 - 4\mu}}{2}\left(\frac{A\cosh\left(z\Big/2\sqrt{\lambda^2 - 4\mu}\right) + B\sinh\left(z\Big/2\sqrt{\lambda^2 - 4\mu}\right)}{A\sinh\left(z\Big/2\sqrt{\lambda^2 - 4\mu}\right) + B\cosh\left(z\Big/2\sqrt{\lambda^2 - 4\mu}\right)}\right)\right)\right\} \times e^{ip} \tag{8}$$

(ii) When $\lambda^2 - 4\mu < 0$thus following trigonometric solutions are obtained.

$$\psi_2(x,t) = \left\{ \frac{\sqrt{-2\phi(x) + 4vp_1 - 2p_2 + 12p_1^2}\left(3\phi(x)\lambda - 18p_1^2\lambda - 6vp_1\lambda + 3p_2\lambda - 2\phi'(x)\right)}{6\phi(x) - 12vp_1 + 6p_2 - 36p_1^2} + \sqrt{-2\phi(x) + 4vp_1 - 2p_2 + 12p_1^2} \times \left(-\frac{\lambda}{2} + \frac{\sqrt{\lambda^2 - 4\mu}}{2}\left(\frac{-A\sin\left(z\Big/2\sqrt{\lambda^2 - 4\mu}\right) + B\cos\left(z\Big/2\sqrt{\lambda^2 - 4\mu}\right)}{A\cos\left(z\Big/2\sqrt{\lambda^2 - 4\mu}\right) + B\sin\left(z\Big/2\sqrt{\lambda^2 - 4\mu}\right)}\right)\right)\right\} \times e^{ip} \tag{9}$$

(iii) When $\lambda^2 - 4\mu = 0$thus following plane solutions are obtained.

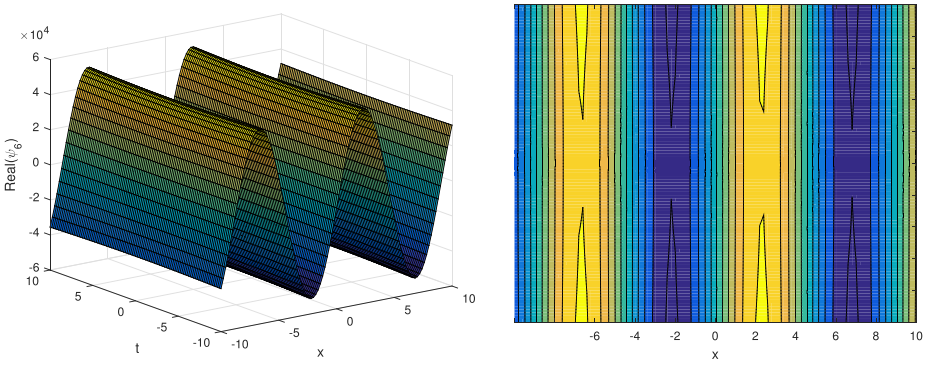

Fig. 23. The 3D plot and the corresponding contour representation of the traveling wave solutions $\psi_6(x,t)$ for different values of parameters.

$$\psi_3(x,t)=\left(-\frac{\lambda}{2}+\frac{B}{A+Bz}\right)\times e^{ip} \tag{10}$$

where

In particular, if $A\to 0$and $B\neq 0$ and $\lambda>0$ then the solution Eq. (8)

The graph and its corresponding contour plot of the solutions $\psi_1(x,t)$ are shown in Fig. 20, for the values of parameters $\rho_1=700,\rho_2=0.0008$, $\lambda=0.05,\mu=0.001,A=0.001,B=50,\phi(x)=sin(x)$ and $\nu=0.02$

The graph and its corresponding contour plot of the solutions $\psi_2(x,t)$

$$z=x-\frac{1}{6(4\mu-\lambda^2)p_1}\Big(12\phi(x)\mu-3\phi(x)\lambda^2+18p_1^2\lambda^2-3p_2p_1^2+12p_2\mu-3p_2\lambda^2+3-72p_1^2\mu+3p_1^4+3\phi(x)p_1^2$$
$$-\left(9-18p_2p_1^2+18\phi(x)p_1^2+48\mu(\phi'(x))^2-12\lambda^2(\phi'(x))^2-18p_1^6p_2+9p_1^4(\phi(x))^2+18p_1^6\phi(x)+9p_1^4p_2^2+9p_1^8-18p_1^4\phi(x)p_2+18p_1^4\right)^{1/2}\Big)t.$$

converges to

$$\psi_4(x,t)=\left\{\frac{\sqrt{-2\phi(x)+4vp_1-2p_2+12p_1^2}\left(3\phi(x)\lambda-18p_1^2\lambda-6vp_1\lambda+3p_2\lambda-2\phi'(x)\right)}{6\phi(x)-12vp_1+6p_2-36p_1^2}\right.$$
$$\left.+\sqrt{-2\phi(x)+4vp_1-2p_2+12p_1^2}\left(-\frac{\lambda}{2}+\frac{\sqrt{\lambda^2-4\mu}}{2}\tanh\left(\frac{z}{2}\sqrt{\lambda^2-4\mu}\right)\right)\right\}$$
$$\times e^{ip}. \tag{11}$$

Also, if $B\to 0$and $A\neq 0$and $\lambda>0$then the solution Eq. (8) converges to

$$\psi_5(x,t)=\left\{\frac{\sqrt{-2\phi(x)+4vp_1-2p_2+12p_1^2}\left(3\phi(x)\lambda-18p_1^2\lambda-6vp_1\lambda+3p_2\lambda-2\phi'(x)\right)}{6\phi(x)-12vp_1+6p_2-36p_1^2}\right.$$
$$\left.+\sqrt{-2\phi(x)+4vp_1-2p_2+12p_1^2}\left(-\frac{\lambda}{2}+\frac{\sqrt{\lambda^2-4\mu}}{2}\coth\left(\frac{z}{2}\sqrt{\lambda^2-4\mu}\right)\right)\right\}$$
$$\times e^{ip}. \tag{12}$$

are shown in Fig. 21, for the values of parameters $\rho_1=700,\rho_2=0.0008$, $\lambda=0.05,\mu=0.001,A=0.001,B=50,\phi(x)=sin(x)$ and $\nu=0.02$.

The graph and its corresponding contour plot of the solutions $\psi_4(x,t)$ are shown in Fig. 22, for the values of parameters $\rho_1=700,\rho_2=0.0008$, $\lambda=0.05,\mu=0.001,A=0.001,B=50,\phi(x)=sin(x)$ and $\nu=0.02$.

For Case-2; The v is free parameter while along with $\beta_0=0$, $\beta_1=\frac{1}{5}\sqrt{-20\frac{\phi'(x)}{\lambda}},\beta_2=\frac{4\phi'(x)\sqrt{-20\frac{\phi'(x)}{\lambda}}\lambda}{\left((-60\lambda^2+80\mu)\phi'(x)+25\lambda\left(p_1{}^4+1-p_2p_1^2+\phi(x)p_1^2\right)\right)}$,

$$v=\frac{-30p_1^2\lambda+5\phi(x)\lambda+5p_2\lambda-2\phi'(x)}{10p_1\lambda},$$

The constraint condition holds for the following results, when v is putting in it,

$$\lambda=-\frac{2\phi'(x)}{40p_1^2+15\phi(x)+15p_2}$$

(i) When $\lambda^2-4\mu>0$thus following families of hyperbolic solutions

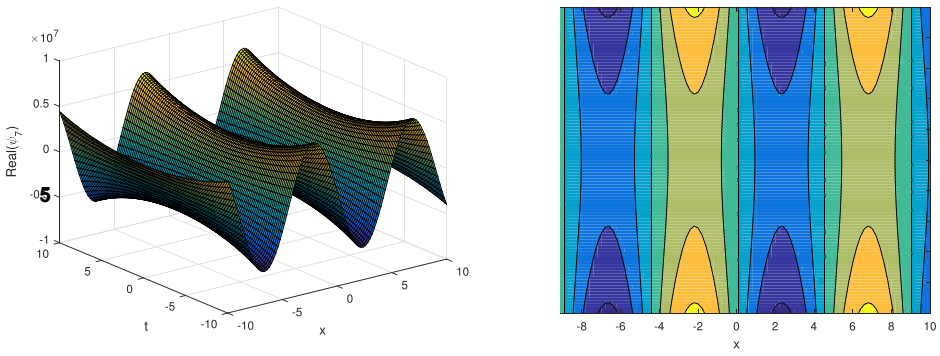

Fig. 24. The 3D plot and the corresponding contour representation of the traveling wave solutions $\psi_7(x,t)$ for different values of parameters.

are obtained.

$$\psi_5(x,t)=\left\{\frac{2}{5}\sqrt{\frac{-5\phi'(x)}{\lambda}}\left(-\frac{\lambda}{2}+\frac{\sqrt{\lambda^2-4\mu}}{2}\left(\frac{A\cosh\left(1/2z\sqrt{\lambda^2-4\mu}\right)+B\sinh\left(1/2z\sqrt{\lambda^2-4\mu}\right)}{A\sinh\left(1/2z\sqrt{\lambda^2-4\mu}\right)+B\cosh\left(1/2z\sqrt{\lambda^2-4\mu}\right)}\right)\right)\right.$$
$$+8\phi'(x)\sqrt{\frac{-5\phi'(x)}{\lambda}}\lambda\left(-\frac{\lambda}{2}+\frac{\sqrt{\lambda^2-4\mu}}{2}\left(\frac{A\cosh\left(1/2z\sqrt{\lambda^2-4\mu}\right)+B\sinh\left(1/2z\sqrt{\lambda^2-4\mu}\right)}{A\sinh\left(1/2z\sqrt{\lambda^2-4\mu}\right)+B\cosh\left(1/2z\sqrt{\lambda^2-4\mu}\right)}\right)\right)^2\left(\left(-60\lambda^2+80\mu\right)\phi'(x)+25\lambda\left(p_1{}^4+1\right.\right.$$
$$\left.\left.\left.-p_2p_1^2+\phi(x)p_1^2\right)\right)^{-1}\right\}\times e^{ip}. \tag{13}$$

If $A\to 0$and $B\neq 0$and $\lambda>0$then the solution Eq. (13) converges to

$$\psi_6(x,t)=\left\{\frac{2}{5}\sqrt{\frac{-5\phi'(x)}{\lambda}}\left(-\frac{\lambda}{2}+\frac{\sqrt{\lambda^2-4\mu}}{2}\tanh\left(\frac{1}{2}z\sqrt{\lambda^2-4\mu}\right)\right)\right\}+$$
$$8\phi'(x)\sqrt{\frac{-5\phi'(x)}{\lambda}}\lambda\left(-\frac{\lambda}{2}+\frac{\sqrt{\lambda^2-4\mu}}{2}\tanh\left(\frac{1}{2}z\sqrt{\lambda^2-4\mu}\right)^2\right)$$
$$\left(\left(-60\lambda^2+80\mu\right)\phi'(x)+25\lambda\left(p_1{}^4+1-p_2p_1^2+\phi(x)p_1^2\right)\right)^{-1}\Big\}\times e^{ip}. \tag{14}$$

Also, if $B\to 0$ and $A\neq 0$and $\lambda>0$ then the solution Eq. (13) converges to

$$\psi_7(x,t)=\left\{\frac{2}{5}\sqrt{\frac{-5\phi'(x)}{\lambda}}\left(-\frac{\lambda}{2}+\frac{\sqrt{\lambda^2-4\mu}}{2}\tanh\left(\frac{1}{2}z\sqrt{\lambda^2-4\mu}\right)\right)\right\}+$$
$$8\phi'(x)\sqrt{\frac{-5\phi'(x)}{\lambda}}\lambda\left(-\frac{\lambda}{2}+\frac{\sqrt{\lambda^2-4\mu}}{2}\coth\left(\frac{1}{2}z\sqrt{\lambda^2-4\mu}\right)^2\right)$$
$$\left(\left(-60\lambda^2+80\mu\right)\phi'(x)+25\lambda\left(p_1{}^4+1-p_2p_1^2+\phi(x)p_1^2\right)\right)^{-1}\Big\}\times e^{ip}. \tag{15}$$

(ii) When $\lambda^2-4\mu<0$thus following trigonometric wave solution are obtained.

$$\psi_8(x,t)=\left\{\frac{2}{5}\sqrt{\frac{-5\phi'(x)}{\lambda}}\left(-\frac{\lambda}{2}+\sqrt{4\mu-\lambda^2}\left(\frac{-A\sin\left(1/2z\sqrt{4\mu-\lambda^2}\right)+B\cos\left(1/2z\sqrt{4\mu-\lambda^2}\right)}{A\cos\left(1/2z\sqrt{4\mu-\lambda^2}\right)+B\sin\left(1/2z\sqrt{4\mu-\lambda^2}\right)}\right)\right)\right.$$
$$+8\phi'(x)\sqrt{\frac{-5\phi'(x)}{\lambda}}\lambda\left(-\frac{\lambda}{2}+\sqrt{4\mu-\lambda^2}\left(\frac{-A\sin\left(1/2z\sqrt{4\mu-\lambda^2}\right)+B\cos\left(1/2z\sqrt{4\mu-\lambda^2}\right)}{A\cos\left(1/2z\sqrt{4\mu-\lambda^2}\right)+B\sin\left(1/2z\sqrt{4\mu-\lambda^2}\right)}\right)\right)^2\left(\left(-60\lambda^2+80\mu\right)\phi'(x)+25\lambda\left(p_1{}^4\right.\right.$$
$$\left.\left.\left.+1-p_2p_1^2+\phi(x)p_1^2\right)\right)^{-1}\right\}\times e^{ip}. \tag{16}$$

(iii) When $\lambda^2-4\mu=0$thus plane solution are obtained.

$$\psi_9(x,t)=\left(-\frac{\lambda}{2}+\frac{B}{A+Bz}\right)\times e^{ip} \tag{17}$$

where

$$z=x-\left(\frac{-30p_1^2\lambda+5\phi(x)\lambda+5p_2\lambda-2\phi'(x)}{10p_1\lambda}\right)t \tag{18}$$

The graph and its corresponding contour plot of the solutions $\psi_6(x,t)$ are shown in Fig. 23, for the values of parameters $\rho_1=0.7,\rho_2=0.008,\lambda=0.05,\mu=0.09,A=10,B=0.005,\phi(x)=sin(x)$ and $\nu=0.2$

The graph and its corresponding contour plot of the solutions $\psi_7(x,t)$ are shown in Fig. 24, for the values of parameters $\rho_1=0.7,\rho_2=0.008,\lambda=0.05,\mu=0.09,A=10,B=0.005,\phi(x)=sin(x)$ and $\nu=0.2$.

For Case-3: The β_1 is free parameter while along with $\beta_0=\beta_0$, $\beta_2=0$, $\beta_1=-2\frac{\phi(x)-2\nu\rho_1-6p_1^2+\rho_2}{\beta_0}$,

$$v=-\frac{1}{24\lambda\mu p_1}\left(36\lambda^2\mu^2(\phi(x))^2-432\lambda\left(\left(-1/12p_1-1/6p_2+p_1^2\right)\lambda\right.\right.$$
$$\left.-1/36p_1\right)\mu-1/12p_1\beta_0\Big)\mu\phi(x)-48\lambda\mu p_1\phi'(x)\beta_0$$
$$+1296\left(\left(\left(-1/12p_1-1/6p_2+p_1^2\right)\lambda-1/36p_1\right)\mu-1/12p_1\beta_0\right)^2$$
$$\left.+6\lambda\mu\phi(x)+\left(\left(-3p_1+6p_2-36p_1^2\right)\lambda-p_1\right)\mu-3p_1\beta_0\right)^{1/2}.$$

.

The constraint condition holds for the following results, when $v$is

putting in it,

$$\lambda = -\frac{p_1\left(8\mu p_1^2 + 9\phi(x)\beta_0 + 2\phi^{'}(x)\beta_0 + 24p_1^2\beta_0 + 9p_2\beta_0 + 3\mu\phi(x) + 3\mu p_2\right)}{3\mu\left(8p_1^3 + 24p_2^2 + 32p_1^4 + 24\left(\phi(x)\right)^2 + 76p_2p_1^2 + 3\phi(x)p_1 + 48\phi(x)p_2 + 76\phi(x)p_1^2 + 3p_1p_2\right)}.$$

(i) When $\lambda^2 - 4\mu > 0$ thus following hyperbolic solutions are obtained.

$$\psi_{10}(x,t) = \left\{\beta_0 - \frac{2\left(\phi(x) - 2vp_1 - 6p_1^2 + p_2\right)\left(-\frac{\lambda}{2} + \frac{\sqrt{\lambda^2-4\mu}}{2}\left(\frac{A\cosh\left(1/2\,z\sqrt{\lambda^2-4\mu}\right)+B\sinh\left(1/2\,z\sqrt{\lambda^2-4\mu}\right)}{A\sinh\left(1/2\,z\sqrt{\lambda^2-4\mu}\right)+B\cosh\left(1/2\,z\sqrt{\lambda^2-4\mu}\right)}\right)\right)^2}{\beta_0}\right\} \times e^{ip}. \tag{19}$$

If $A \to 0$ and $B \neq 0$ and $\lambda > 0$, then Eq. (19) becomes

$$\psi_{11}(x,t) = \left\{\beta_0 - \frac{2\left(\phi(x) - 2vp_1 - 6p_1^2 + p_2\right)\left(-\frac{\lambda}{2} + \frac{\sqrt{\lambda^2-4\mu}}{2}\left(\tanh\left(\frac{1}{2}\,z\sqrt{\lambda^2-4\mu}\right)\right)\right)^2}{\beta_0}\right\} \times e^{ip}. \tag{20}$$

Also, if $B \to 0$and $A \neq 0$and $\lambda > 0$, then Eq. (19) becomes

$$\psi_{12}(x,t) = \left\{\beta_0 - \frac{2\left(\phi(x) - 2vp_1 - 6p_1^2 + p_2\right)\left(-\frac{\lambda}{2} + \frac{\sqrt{\lambda^2-4\mu}}{2}\left(\coth\left(\frac{1}{2}\,z\sqrt{\lambda^2-4\mu}\right)\right)\right)^2}{\beta_0}\right\} \times e^{ip}. \tag{21}$$

(ii) When $\lambda^2 - 4\mu < 0$thus following traveling wave solutions are obtained.

$$\psi_{13}(x,t) = \left\{\beta_0 - \frac{2\left(\phi(x) - 2vp_1 - 6p_1^2 + p_2\right)\left(-\frac{\lambda}{2} + \sqrt{4\mu-\lambda^2}\left(\frac{-A\sin\left(1/2\,z\sqrt{4\mu-\lambda^2}\right)+B\cos\left(1/2\,z\sqrt{4\mu-\lambda^2}\right)}{A\cos\left(1/2\,z\sqrt{4\mu-\lambda^2}\right)+B\sin\left(1/2\,z\sqrt{4\mu-\lambda^2}\right)}\right)\right)^2}{\beta_0}\right\} \times e^{ip}. \tag{22}$$

(iii) When $\lambda^2 - 4\mu = 0$thus plane solutions are obtained.

$$\psi_{14}(x,t) = \left(-\frac{\lambda}{2} + \frac{B}{A + Bz}\right) \times e^{ip}. \tag{23}$$

where

$$z = x - \frac{1}{24\lambda\mu p_1}\Big(36\lambda^2\mu^2(\phi(x))^2 - 432\lambda\left(\left(\left(-1/12p_1 - 1/6p_2 + p_1^2\right)\lambda - 1/36p_1\right)\mu - 1/12p_1\beta_0\right)\mu\phi(x) - 48\lambda\mu p_1\phi'(x)\beta_0 + 1296\left(\left(\left(-1/12p_1 - 1/6p_2 + p_1^2\right)\lambda - 1/36p_1\right)\mu - 1/12p_1\beta_0\right)^2 + 6\lambda\mu\phi(x) + \left(\left(-3p_1 + 6p_2 - 36p_1^2\right)\lambda - p_1\right)\mu - 3p_1\beta_0\Big)^{1/2} \times t.$$

Remark

Since the relation between ϕ and ψ is the defined in Eq. (1), so using the definition of Δ operator. The value of ϕ can be obtained by twice integrating to $|\psi|$ w.r.t space variable for above each solutions ψ_i, where $i = 1, 2, 3, \ldots, 25$.

Conclusion

In this article, the diverse exact traveling wave solutions are obtained in the form of hyperbolic, trigonometric and plane wave families. The system under investigation is the Schrodinger–Poisson system which has applications in gravity's role of quantum state. The solutions are constructed using two norms of integration MEDA and (G'/G)-expansion techniques. The constraints conditions for the existence of solutions also emerged during the derivation of solutions. The 3D graphs and their corresponding contour graphs are also being plotted by the proper choice of parameters. The results are new and helpful to compare with numerical results.

CRediT authorship contribution statement

M. Younis: Software, Validation, Supervision. **A.R. Seadawy:** Conceptualization, Methodology. **M.Z. Baber:** Writing - review & editing. **S. Husain:** Writing - review & editing. **M.S. Iqbal:** Data curation, Writing - original draft. **S.T. R. Rizvi:** Visualization, Investigation. **Dumitru Baleanu:** Writing - review & editing.

Declaration of Competing Interest

The authors declare that they have no known competing financial interests or personal relationships that could have appeared to influence the work reported in this paper.

References

[1] Cheemaa N, Younis M. New and more exact traveling wave solutions to integrable (2+ 1)-dimensional maccari system. Nonlinear Dyn 2016;83(3):1395–401.
[2] Nakatsuji H. Discovery of a general method of solving the schrodinger and dirac equations that opens a way to accurately predictive quantum chemistry. Acc Chem Res 2012;45(9):1480–90.
[3] Penrose R. On gravity's role in quantum state reduction. Gen Relat Grav 1996;28 (5):581–600.
[4] Giulini D, Großardt A. The schrödinger–newton equation as a non-relativistic limit of self-gravitating klein–gordon and dirac fields. Class Quant Grav 2012;29(21): 215010.
[5] Aly R. Seadawy, Dipankar Kumar, Anuz Kumar Chakrabarty, Dispersive optical soliton solutions for the hyperbolic and cubic-quintic nonlinear Schrodinger equations via the extended sinh-Gordon equation expansion method. Eur Phys J Plus 2018;133(182):1-12.
[6] Obaidullah U, Jamal S. A computational procedure for exact solutions of burgers' hierarchy of nonlinear partial differential equations. J Appl Math Comput 2020: 1–11.
[7] Zhang R-F, Bilige S. Bilinear neural network method to obtain the exact analytical solutions of nonlinear partial differential equations and its application to p-gbkp equation. Nonlinear Dyn 2019;95(4):3041–8.
[8] Tu KM, Yih KA, Chou FI, Chou JH. Numerical solution and taguchi experimental method for variable viscosity and non-newtonian fluids effects on heat and mass transfer by natural convection in porous media. Int J Comput Sci Eng 2020;22 (2–3):252–61.
[9] Ryabov PN, Sinelshchikov DI, Kochanov MB. Application of the kudryashov method for finding exact solutions of the high order nonlinear evolution equations. Appl Math Comput 2011;218(7):3965–72.
[10] Baldwin D, Göktaş Ü, Hereman W. Symbolic computation of hyperbolic tangent solutions for nonlinear differential–difference equations. Comput Phys Commun 2004;162(3):203–17.
[11] Aslan I. On the application of the exp-function method to the kp equation for n-soliton solutions. Appl Math Comput 2012;219(6):2825–8.
[12] Nikolai A. Kudryashov, Simplest equation method to look for exact solutions of nonlinear differential equations. Chaos Solitons Fract 2005;24(5):1217–31.
[13] Nikolai A. Kudryashov, Exact solitary waves of the fisher equation. Phys Lett Sec A 2005;342(1–2):99–106.
[14] Nikolai A. Kudryashov, One method for finding exact solutions of nonlinear differential equations. Commun Nonlinear Sci Numer Simul 2012;17(6):2248–53.
[15] Kudryashov Nikolai A. Logistic function as solution of many nonlinear differential equations. Appl Math Model 2015;39(18):5733–42.
[16] Shi Y, Dai Z, Li D. The correct traveling wave solutions for the high-order dispersive nonlinear schrödinger equation. Appl Math Comput 2010;216(5): 1583–91.
[17] Wazwaz A-M. The hirota's direct method and the tanh–coth method for multiple-soliton solutions of the sawada–kotera–ito seventh-order equation. Appl Math Comput 2008;199(1):133–8.
[18] Islam W, Younis M, et al. Weakly nonlocal single and combined solitons in nonlinear optics with cubic quintic nonlinearities. J Nanoelectron Optoelectron 2017;12(9):1008–12.
[19] Arshad M, Seadawy Aly, Lu Dianchen. Elliptic function and Solitary Wave solutions of the higher-order nonlinear Schrodinger dynamical equation with fourth-order dispersion and cubic-quintic nonlinearity and its stability. Eur Phys J Plus 2017; 132:371.
[20] Younas U, Seadawy AR, Younis M, Rizvi S. Optical solitons and closed form solutions to the (3+ 1)-dimensional resonant schrödinger dynamical wave equation. Int J Mod Phys B 2020:2050291.
[21] Rehman HU, Younis M, Jafar S, Tahir M, Saleem MS. Optical solitons of biswas-arshed model in birefrigent fiber without four wave mixing. Optik 2020;213: 164669.
[22] Rehman SU, Aly R. Seadawy, Younis, M, Rizviz STR, Sulaiman TA, Yusuf A. Modulation instability analysis and optical solitons of the generalized model for description of propagation pulses in optical fiber with four non-linear terms. Mod Phys Lett B 2021;35(6):2150112 (20 pages).
[23] Conley R, Delaney TJ, Jiao X. A hybrid method and unified analysis of generalized finite differences and lagrange finite elements. J Comput Appl Math 2020:112862.
[24] Jose J, Choi S-J, Giljarhus KET, Gudmestad OT. A comparison of numerical simulations of breaking wave forces on a monopile structure using two different numerical models based on finite difference and finite volume methods. Ocean Eng 2017;137:78–88.
[25] Zhang Y, Xiong A. A particle method based on a generalized finite difference scheme to solve weakly compressible viscous flow problems. Symmetry 2019;11 (9):1086.
[26] Zhang J-K, Dong H, Zhou E-Z, Li B-W, Tian X-Y. A combined method for solving 2d incompressible flow and heat transfer by spectral collocation method and artificial compressibility method. Int J Heat Mass Transf 2017;112:289–99.
[27] Gao Y, Mei L. Galerkin finite element methods for two-dimensional rlw and srlw equations. Appl Anal 2018;97(13):2288–312.
[28] Akbulut Arzu, Almusawa Hassan, Kaplan Melike, Osman MS. On the conservation laws and exact solutions to the (3+ 1)-dimensional modified KdV-Zakharov-Kuznetsov equation. Symmetry 2021;15:756.
[29] Nauman Raza, Muhammad Hamza Rafiq, Melike Kaplan, Sunil Kumar, Yu-Ming Chu. The unified method for abundant soliton solutions of local time-fractional nonlinear evolution equations. Results Phys 2021;22:103979.
[30] Melike Kaplan, Mehmet Naci Ozer. Multiple-soliton solutions and analytical solutions to a nonlinear evolution equation. Opt Quant Electron 2018;50(1):2.
[31] Kaplan Melike, San Sait, Bekir Ahmet. On the exact solutions and conservation laws to the Benjamin-Ono equation. J Appl Anal Comput 2018;8(1):1–9.
[32] Ali Asghar, Seadawy Aly R, Dianchen Lu. Computational methods and traveling wave solutions for the fourth-Order nonlinear Ablowitz-Kaup-Newell-Segur water wave dynamical equation via two methods and its applications. Open Phys 2018; 16:219–26.
[33] Ali Asghar, Seadawy Aly R, Dianchen Lu. New solitary wave solutions of some nonlinear models and their Applications. Adv Diff Eqs 2018;2018(232):1–12.
[34] Arshad M, Seadawy Aly, Dianchen Lu. Bright-Dark Solitary Wave Solutions of generalized higher-order nonlinear Schrodinger equation and its applications in optics. J Electromag Waves Appl 2017;31(16):1711–21.

[35] Iftikhar Ahmed, Aly R. Seadawy, Dianchen Lu. M-shaped rational solitons and their interaction with kink waves in the Fokas-lenells equation. Phys Scr 2019;94: 055205 (7pp).
[36] Cheemaa Nadia, Seadawy Aly R, Chen Sheng. More general families of exact solitary wave solutions of the nonlinear Schrodinger equation with their applications in nonlinear optics. Eur Phys J Plus 2018;133:547.
[37] Glam Ozkan Yesim, Yaşar Emrullah, Seadawy Aly. On the multi-waves, interaction and Peregrine-like rational solutions of perturbed Radhakrishnan–Kundu–Lakshmanan equation. Phys Scr 2020;95(8):085205.
[38] Ijaz Ali, Aly R. Seadawy, Syed Tahir Raza Rizvi, Muhammad Younis, Kashif Ali. Conserved quantities along with Painleve analysis and Optical solitons for the nonlinear dynamics of Heisenberg ferromagnetic spin chains model. Int J Mod Phys B 2020;34(30):2050283 (15 pages).
[39] Rizvi STR, Seadawy Aly R, Ashraf F, Younis M, Iqbal H. Dumitru Baleanu, Lump and Interaction solutions of a geophysical Korteweg–de Vries equation. Res Phys 2020;19:103661.
[40] Younis M, Rizvi STR. Dispersive dark optical soliton in (2+ 1)-dimensions by g'/g-expansion with dual-power law nonlinearity. Optik 2015;126(24):5812–4.
[41] Younis M, ur Rehman H, Iftikhar M. Travelling wave solutions to some time–space nonlinear evolution equations. Appl Math Comput 2014;249:81–8.
[42] Farah N, Seadawy AR, Ahmad S, Rizvi STR, Younis M. Interaction properties of soliton molecules and painleve analysis for nano bioelectronics transmission model. Opt Quant Electron 2020;52(7):1–15.